Laser-Matter Interaction in Dielectrics: Insight from Picosecond-Pulsed Second-Harmonic Generation in Periodically Poled $LiTaO_3$

Oleg A. Louchev,[1,*] Satoshi Wada,[1] and Vladislav Ya. Panchenko[2]

[1]*Center for Advanced Photonics, RIKEN, 2-1 Hirosawa, Wako, Saitama 351-0198, Japan*
[2]*Federal Scientific Research Centre "Crystallography and Photonics" of Russian Academy of Sciences, Leninsky pr. 59, Moscow 119333, Russia*

(Received 25 January 2017; revised manuscript received 28 June 2017; published 25 August 2017)

We develop a modified two-temperature (2T) model of laser-matter interaction in dielectrics based on experimental insight from picosecond-pulsed high-frequency temperature-controlled second-harmonic (515 nm) generation in periodically poled stoichiometric $LiTaO_3$ crystal and required for computational treatment of short-pulsed nonlinear optics and materials processing applications. We show that the incorporation of an extended set of recombination-kinetics-related energy-release and heat-exchange processes following short-pulsed photoionization by two-photon absorption of the second harmonic allows accurate simulation of the electron-lattice relaxation dynamics and electron-lattice temperature evolution in $LiTaO_3$ crystal in nonlinear laser-frequency conversion. Our experimentally confirmed model and detailed simulation study show that two-photon ionization with the recombination mechanism via ion-electron-lattice interaction followed by a direct transfer of the recombination energy to the lattice is the main laser-matter energy-transfer pathway responsible for the majority of the crystal lattice heating (approximately 90%) continuing for approximately 50 ps after laser-pulse termination and competing with effect of electron-phonon energy transfer from the free electrons. This time delay is due to a recombination bottleneck which hinders faster relaxation to thermal equilibrium in photoionized dielectric crystal. Generally, our study suggests that in dielectrics photoionized by short-pulsed radiation with intensity range used in nonlinear laser-frequency conversion, the electron-lattice relaxation period is defined by the recombination-stage bottleneck of a few tens of picoseconds and not by the time of the electron-phonon energy transfer. This modification of the 2T model can be applied to a broad range of processes involving laser-matter interactions in dielectrics and semiconductors for charge density reaching the range of 10^{21}–10^{22} cm^{-3}.

DOI: 10.1103/PhysRevApplied.8.024025

I. INTRODUCTION

Nonlinear laser-frequency conversion is a constantly growing field of optical technology encompassing a wide range of applications, input and generated laser frequencies, laser intensities and pulse durations, repetition rates, nonlinear materials, and media [1]. The last two decades of the development of this field have been marked by a technical breakthrough in production of periodically poled (PP) crystal structures [2] allowing practical operation under low temperatures [3] by using quasi-phase-matching of the laser waves as suggested in classical work [4]. Significant progress in practical application of nonlinear PP crystal structures has occurred in recent years [5], leading step by step towards greater efficiency operation at higher input intensities. However, high-intensity and short-pulsed operation in nonlinear laser-frequency conversion is associated with a number of side effects and limitations induced by the input and generated laser waves.

In this connection, the progress in development, optimization, and applications of high-efficiency nonlinear optical devices can be effectively supported by the development of theoretical and application-oriented computational models allowing a complex multiscale analysis of the main laser-frequency conversion mechanism in the presence of various laser-induced side effects.

The formalization of the applied computational models of nonlinear laser-frequency conversion including the various effects caused by laser-induced heating and plasma generation depends on laser-pulse duration. That is, in the interaction of nanosecond laser pulses with nonlinear optical crystals, the temperature of the electron-lattice system is assumed to be in quasiequilibrium after fast electron-lattice relaxation, allowing the use of the heat-conduction equation for estimating the temperature- related thermo-optical effects crucial for laser-beam propagation and laser-frequency conversion [6–8]. In contrast, during laser-matter interaction of picosecond- and shorter pulse duration, the relaxation time is larger than the pulse duration, and the temperature of excited free electrons differs from that of the lattice. In this case, the complex

*oleglouchev@riken.jp

process of electron-lattice energy exchange and relaxation to the equilibrium is described by the two-temperature (2T) model developed initially to treat the relaxation between electrons and crystalline lattices [9]. This 2T model approach was then adopted as a reliable theoretical framework for short-pulsed laser-matter interaction in metals, semiconductors, and dielectrics [10–14] providing valuable insights into many materials processing applications under intensive short-pulsed laser radiation [15]. In particular, the 2T model and related simulation form a significant part of the theoretical framework underpinning the recent study revealing large optical nonlinearity in indium tin oxide [16].

Short-pulsed laser-matter interaction has remained the focus of many research papers using various experimental approaches and theoretical models for the estimation of laser-light absorption, electron and lattice temperature for the laser ablation process, surface and bulk damage, modification of optical properties of dielectric materials, and electron-lattice relaxation in photoexcited materials [10–31]. Our present work focuses on a modification of the phenomenological 2T model of laser-matter interaction for short-pulsed operation in nonlinear optical materials and is based on a recent experimental study of the temperature-controlled picosecond-pulsed second-harmonic generation (SHG) by a periodically poled stoichiometric $LiTaO_3$ (PPSLT) crystal [32]. In this paper, we develop a modified 2T model which extends the theoretical framework of laser-matter interaction allowing comprehensive simulation of the underlying mechanism of short-pulsed photoionization followed by electron-lattice relaxation and lattice heating in a SHG experiment yielding good agreement of the simulations with the experimental data.

In particular, in treating the case of short-pulsed laser-matter interaction in nonlinear laser-frequency conversion [32], we first consider in detail the experimental data of temperature-controlled high-frequency picosecond SHG in PP $LiTaO_3$ from which we find the value of the lattice temperature increase resulting from a single laser pulse. After that, we introduce a modification to the 2T model allowing the calculation of all parameters which may be significant for laser-beam frequency conversion and propagation in nonlinear optical devices: charge density, electron energy (temperature), and lattice temperature. We make a detailed computational study to evaluate the effect of the main important parameters. In particular, we study the effect of the electron-phonon energy-transfer rate constant with resulting energy of free electrons and dynamics of recombination mechanism. Additionally, we discuss when this modification can be used in other cases of short-pulsed laser-matter interaction.

In Sec. II, we discuss the experimental data of high-frequency picosecond-pulsed SHG. In Sec. III, we develop the modified 2T model. In Sec. IV, we give the results of (i) the reduced analytical approximation and (ii) the comprehensive simulation of the experimental case given in Sec. II. In Sec. V, we discuss applying the modified model to other cases of short-pulsed laser-matter interaction. In Sec. VI, we give a short summary of our work.

II. EXPERIMENT AND DATA ANALYSIS

We use the experimental data of picosecond-pulsed SHG by the temperature-controlled quasi-phase-matching (QPM) of PPSLT crystal [32]. In particular, in Fig. 1 we show the measured SHG efficiency as a function of input peak intensity $I_1 = 0.1$–9.5 GW/cm^2 using (i) 2-mm-long crystal, (ii) $\lambda_1 = 1030$ nm pulsed input radiation of $\tau_p = 18$ ps pulse duration, (iii) $\nu_p = 10$ kHz pulse repetition rate, (iv) $\sqrt{2}r_0 = 0.15$ mm input beam radius, and (v) QPM temperature $T_{\mathrm{QPM}} = 41$°C.

The red line in Fig. 1 shows SHG efficiency η vs I_1 measured during operation with the temperature of the crystal holder T_c maintained at the QPM temperature, $T_c = T_{\mathrm{QPM}} = 41$°C. This line shows the increase and saturation of SHG efficiency at the level of $\eta \approx 0.35$ followed by its decrease towards $\eta = 0.22$ associated with thermally induced dephasing [32]. The black line shows the SHG efficiency η vs I_1 measured during operation with the crystal holder maintained at 10 K below that of QPM:$T_C = T_{\mathrm{QPM}} - 10 = 31$ °C. These data show how the thermal dephasing caused by the absorption of the second harmonic revealed in the first case can be compensated by a temperature shift $\Delta T_{\mathrm{exp}} \approx 10$ K allowing one to restore SHG efficiency to the maximal possible level $\eta \approx 0.35$ with $I_1 = 9.5$ GW/cm^2.

We use these experimental data for estimating the value of temperature increase for a single pulse by considering several analytical expressions [33,34]. The experimental value of the optimal temperature shift ($\Delta T_{\mathrm{exp}} = T_{\mathrm{QPM}} - T_c \approx 10$ K) found in Fig. 1 for efficiency recovery under $I_1 = 9.5$ GW/cm^2 corresponds to the maximum of the temperature tolerance curve of SHG at $T_{\mathrm{QPM}} = 41$°C and, hence, to 50% of the maximal temperature increase

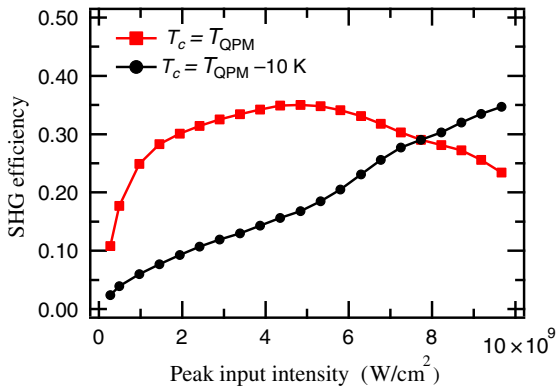

FIG. 1. Experimental data for SHG by PPSLT: SHG efficiency vs peak input intensity.

induced in the operating crystal, approximately $\Delta T_{SP} S_N$, where ΔT_{SP} is the single-pulse temperature increase and $S_N = \sum_{n=1}^{N} \exp[-nD_T/(2\nu_P r_0^2)]$ is the multipulse thermal superposition factor [33,34] taking into account the heat dissipation, where $D_T = 2.01 \times 10^{-2}$ cm^2/s [35] is the heat diffusivity of $LiTaO_3$ and N is the number of pulses. Therefore, by using $\Delta T_{exp} \approx 0.5 \Delta T_{SP} S_N \approx 10$ K, we can find the following value for the single-pulse temperature increase:

$$\Delta T_{SP} \approx 2\Delta T_{exp}/S_N \approx 0.18 \text{ K}, \quad (1)$$

where $S_N \approx 111.5$ for $N \to \infty$, $\nu_p = 10$ kHz, and $\sqrt{2} r_0 = 0.15$ mm.

By using this value, we obtain simplified estimates of the related absorption effects. Assuming that (i) the thermal effect is mainly associated with the recombination of all free electrons with energy release per one electron equivalent to the energy band gap $E_g = 4.6$ eV of $LiTaO_3$ and (ii) the energy of free electrons $\varepsilon_e \ll E_g$, we can estimate the number of free electrons generated during the single pulse Δn_e as [31]

$$\Delta n_e \approx \Delta T_{SP} \rho C / E_g \approx 7.4 \times 10^{17} \text{ cm}^{-3}, \quad (2)$$

and the photoionization (PI) frequency as

$$w_{PI} = \Delta n_e / (\tau_P N^*) \approx 2.14 \times 10^6 \text{ s}^{-1}, \quad (3)$$

where $\rho = 7400$ kg/m^3 is the density, $C = 410$ J/kg K is the specific heat, $N^* = \rho/M \approx 1.9 \times 10^{22}$ cm^{-3} is the molecular density, and $M = 236$ a.u. is the molecular mass of the $LiTaO_3$ crystal.

By using these values, we can get an estimate of the related absorption coefficient as follows: approximately $-(1/I_2)[(dI_2)/dz] \approx [(\Delta n_e E_g)/I_2 \tau_P] \approx 9.1$ cm^{-1} for SH intensity $I_2 = \eta I_1 = 0.35 \times 9.5 = 3.32$ GW/cm^2. This value is much larger than the absorption coefficients associated with the generated free electrons estimated as follows: $\alpha_{e-1} = [(\nu_{e\text{-ph}}^{mom}/c)][(\omega_p^2)/\omega_1^2] \approx 0.26$ cm^{-1} and $\alpha_{e-2} = [(\nu_{e\text{-ph}}^{mom}/c)[(\omega_p^2)/\omega_2^2] \approx 0.065$ cm^{-1}, where $\nu_{e\text{-ph}}^{mom} \approx k_B T/\hbar \approx 4.1 \times 10^{13}$ Hz is the electron-phonon momentum-transfer rate (collision frequency), $\omega_1 = 1.83 \times 10^{15}$ rad/s for the input 1030-nm radiation, $\omega_2 = 3.66 \times 10^{15}$ rad/s for the generated SH of 515 nm, $c = 3 \times 10^8$ m/s, and ω_P is the plasma frequency defined as follows: $\omega_P = e(n_e/\epsilon_0 m_e)^{1/2}$, where e is the electron charge, ϵ_0 is the vacuum permittivity, m_e is the electron mass, and $n_e \approx 2 \times 10^{17}$ cm^{-3} is the maximal electron density achieved during the pulse (see Sec. IV).

Let us now estimate the temperature increase associated with two-photon absorption (TPA) by using the following expression for the TPA coefficient:

$$\beta_{TPA} \approx 2\sigma^{(2)} N^*/\hbar\omega_2 \approx 2.5 \text{ cm/GW}, \quad (4)$$

where $\hbar$ is the Dirac constant, and $\sigma^{(2)} \approx 2.5 \times 10^{-50}$ cm^4 s/photon^2 is the estimate of the TPA cross section ($\lambda_2 = 515$ nm) [1].

This value agrees well with the experimentally defined range for the TPA coefficient 1.1–2.7 cm/GW [32], and by neglecting the thermal energy dissipation by heat diffusion during electron-lattice relaxation, we can estimate the temperature increase after a single laser pulse via the value of generated pulse energy $Q_2 = \eta Q_1$ as follows:

$$\Delta T_{SP} \approx \frac{\beta_{TPA} I_2^2 \tau_P}{\rho C} \approx 0.16 \text{ K}, \quad (5)$$

where $\tau_p \approx 18$ ps, $I_2 = Q_2/(2\pi r_0^2 \tau_p) \approx 3.32$ GW/cm^2, and $\eta \approx 0.35$ (see Fig. 1).

This estimate agrees well with that of Eq. (1) and suggests that in this experiment the lattice heating mechanism can be mainly attributed to the effect of the TPA of the generated second harmonic.

Let us roughly estimate how changing the laser intensity during the pulse can affect the final values of ΔT_{SP} and Δn_e. The ionizing laser intensity is expressed as $I_2(t) \approx I_{2-0} \exp(-2t^2/\tau'^2)$, where $\tau' = \tau_p/2$, and $I_{2-0} = 2^{1/2} Q_2/(\pi^{3/2} r_0^2 \tau_p)$ is the peak intensity of the second harmonic scaled to provide the generated SH pulse energy $Q_2 = \eta Q_1$ by integration of $I_2(t)$ over time and beam radius. After integrating $\rho C dT/dt \approx \beta_{TPA} I_2^2(t)$, the related temperature effect is determined by $2\Delta T_{SP}/\sqrt{\pi}$, where ΔT_{SP} is given by Eq. (5). That is, assuming a constant laser intensity in the calculations can lead to $(2/\sqrt{\pi} - 1) \times 100 \approx 13\%$ errors in estimating the values of the generated temperature effect and related electron density.

III. 2T MODEL

Let us now consider the 2T model for short-pulsed laser-matter interaction in nonlinear optical crystals on the time scale of relaxation between laser-induced free electrons and the crystal lattice. Generally, in treating this problem, two interacting subsystems are considered: (i) the free electrons generated into the conduction band with a density of n_e and the related thermal energy density $E_e = n_e \varepsilon_e = n_e C_e T_e$ (T_e is the electron temperature, $\varepsilon_e = C_e T_e$ is the electron energy, and $C_e = 3k_B/2$ is the specific heat of the electron gas), and (ii) the lattice with related atomic density n_L and thermal energy $E_L = n_L C_L T_L$ (T_L is the lattice temperature $n_L = N^*$ and $n_L C_L = \rho C$). We neglect in our study the impact ionization by high-energy electrons assuming that the value of ε_e remains below the critical energy necessary for this type of ionization.

First, in considering how under photoionization the electron energy density evolves with time, we take into

account the rate of photoionization (PI) $W_{\mathrm{PI}} = w_{\mathrm{PI}} N^*$ and related contribution to the energy-density rate of the electron subsystem as $W_{\mathrm{PI}}(n_{\mathrm{ph}}\hbar\omega_2 - E_g)$, where n_{ph} is the number of photons required for ionization. Second, we take into account that the free electrons can be heated by the laser waves with a rate given by $n_e \sum 2\varepsilon_{\mathrm{qi}}\, \nu^{\mathrm{mom}}_{e\text{-ph}}$, where the sum $\sum$ takes into account both laser frequencies involved in nonlinear laser-frequency conversion, $\varepsilon_{\mathrm{qi}} = [(e^2E_i^2)/4m_e\omega_i^2]$ is the electron quiver energy, and E_i is the electric field amplitude of the related laser wave. Third, in ferroelectric materials the free electrons can also be accelerated by the quasiconstant electrostatic field E induced across the irradiated zone by charge separation, local perturbation in the lattice temperature, and spontaneous polarization. The rate of this effect follows from the Newton equation ($m_e dV_e/dt = eE$) and is given by $\sqrt{2}en_e|E|\varepsilon_e^{1/2}/m_e^{1/2}$. Fourth, we take into account the energy transfer between the two subsystems, i.e., $\nu^{\mathrm{en}}_{e\text{-ph}} n_e C_e (T_e - T_L)$, where $\nu^{\mathrm{en}}_{e\text{-ph}} = 1/\tau^*$ is the electron-phonon energy-transfer rate, and $\tau^* \approx 1$–7 ps is the related characteristic energy-transfer time [15,28,36,37].

Let us now consider the recombination kinetics and related energy-exchange effects outlining the main modification point suggested in our work. In particular, under generation of plasma in materials, the recombination can be treated as a triple-collision effect. First, one can consider the triple collision involving one ion and two free electrons and occurring with the rate of $\beta_R n_i n_e^2$, where β_R is the Auger recombination constant, and n_i and n_e are the density of ions and electrons, respectively. This pathway of recombination is considered in 2T models for photoexcited semiconductors using the experimental value of $\beta_R = 3.8 \times 10^{-31}$ cm^6/s found for Si [38]. In this case, the recombination energy (equivalent to E_g) is released after the ion captures one free electron and is transferred together with the energy of the captured free electron $\varepsilon_e = C_e T_e$ to the second free electron remaining in the conduction band. That is, in this case, the energy of $E_g + \varepsilon_e$ per one collision feeds first the energy of the electron subsystem, and only after that, it is transferred to the lattice by electron-phonon (e-ph) energy transfer, i.e., by the above-mentioned $\nu^{\mathrm{en}}_{e\text{-ph}} n_e C_e (T_e - T_L)$. Consequently, in the related 2T model, the product of (i) the recombination rate and the (ii) electron and recombination energy, i.e., $\beta_R n_i n_e^2 (E_g + \varepsilon_e)$, is introduced into the energy rate equation for the electron subsystem. Thus, in this case, before being transferred to the crystal lattice, all radiation energy absorbed by the photoionization accumulates in the electronic subsystem.

However, in contrast with the above-mentioned pathway of recombination, one can consider that in wide band-gap optical materials, the recombination proceeds by the triple collision involving one ion, one electron, and one neighboring lattice atom followed by energy transfer directly to the crystal lattice [28]. The rate of this recombination process is given by $p\gamma_R n_i n_e$, where the electron-ion collision constant γ_R depends on the mean electron velocity V_e (or on the electron energy $\varepsilon_e = C_e T_e = 3k_B T_e/2$) as follows: $\gamma_R \approx \sigma_R V_e \approx \sigma_R (2\varepsilon_e/m_e)^{1/2}$, where $\sigma_R \approx 2 \times 10^{-14}$ cm^2 is the Coulomb cross section for the electron-ion collision [39], and $p \approx 1$ is the probability of the lattice atom being present in the vicinity of the location of electron-ion recombination [28]. In this case, the recombination energy together with the energy of the captured free electron $E_g + \varepsilon_e$ feeds directly into the energy of the lattice subsystem. Consequently, in our present work, we treat the effect of recombination energy transfer by using the product of the recombination rate and accompanying energy effects directly in both energy rate equations as (i) the energy loss rate of the electron subsystem $-\gamma_R n_i n_e \varepsilon_e$ and as (ii) the corresponding energy-release rate $\gamma_R n_i n_e (E_g + \varepsilon_e)$ introduced into the energy rate equation for the lattice subsystem. Unlike the previous case, given the same level of charge density reached during photoionization, this mechanism provides significantly lower energy transfer to the electron subsystem, resulting in significantly lower electron energy reached during the pulse.

Thus, in our present work, we consider two recombination pathways and rates defined as follows: (i) $\beta_R n_i n_e^2$ with related energy-transfer rate $\beta_R n_i n_e^2 (E_g + \varepsilon_e)$ and (ii) $\gamma_R n_i n_e$ with related energy-transfer rates $-\gamma_R n_i n_e \varepsilon_e$ and $\gamma_R n_i n_e (E_g + \varepsilon_e)$. Finally, we use the following set of equations:

$$\begin{aligned}
&\frac{\partial (n_e C_e T_e)}{\partial t} + \nabla q_e \\
&= W_{\mathrm{PI}}(n_{\mathrm{ph}}\hbar\omega_2 - E_g) + n_e \sum 2\varepsilon_{\mathrm{qi}}\, \nu^{\mathrm{mom}}_{e\text{-ph}} + bn_e|E|(C_e T_e)^{1/2} \\
&\quad + \beta_R n_i n_e^2 (E_g + C_e T_e) - \gamma_R n_i n_e C_e T_e \\
&\quad - \nu^{\mathrm{en}}_{e\text{-ph}} n_e C_e (T_e - T_L), \qquad (6)
\end{aligned}$$

$$\begin{aligned}
&\frac{\partial (n_L C_L T_L)}{\partial t} + \nabla q_L \\
&\quad = \nu^{\mathrm{en}}_{e\text{-ph}} n_e C_e (T_e - T_L) + \gamma_R n_i n_e (E_g + C_e T_e), \qquad (7)
\end{aligned}$$

where $b = 2^{1/2} e/m_e^{1/2}$, and q_e and q_L are the energy-transport terms for the electrons and lattice subsystems, correspondingly, the effect of which can be neglected for picosecond-pulse duration.

The densities of free electrons and ions are defined by the two following equations:

$$\partial n_e/\partial t + \nabla j_e = W_{\mathrm{PI}} - \beta_R n_i n_e^2 - \gamma_R n_i n_e, \qquad (8)$$

$$\partial n_i/\partial t = W_{\mathrm{PI}} - \beta_R n_i n_e^2 - \gamma_R n_i n_e\ , \qquad (9)$$

where $j_e = -D_e\nabla n_e - \mu E n_e$ is the electron flux density, $\mu \approx 1$–$10\ \mathrm{cm^2/Vs}$ is the electron mobility, and $D_e = \mu k_B T_e/e$ is the diffusion coefficient of electrons.

The electrostatic field E caused by (i) the charge-separation effect and (ii) local change of the spontaneous polarization P_s is defined by the Maxwell equation written for ferroelectric materials as follows:

$$\nabla(\epsilon\epsilon_0 E + P_s) = e(n_i - n_e), \tag{10}$$

where $\epsilon = \epsilon_{33} = 43$ is the relative permittivity for $LiTaO_3$, and the spontaneous polarization depends on the lattice temperature as $P_s = P_{s0} + p_T\Delta T_L$ (with $p_T = dP_s/dT_L = -230\times10^{-6}\ \mathrm{Co/m^2K}$ for $LiTaO_3$) giving the pyroelectric (PE) field when the lattice temperature changes.

Equations (6)–(10) encompass a wide range of possible processes and materials. However, in the particular experimental case of SHG in PPSLT considered here, we find that Auger recombination involving an ion and two electrons does not play a significant role. Consider the triple interaction by assuming that one free electron collides with an ionized molecule which has already in its vicinity a second free electron. In this case, the related rate of recombination can be estimated as $p^*\sigma_R^* V_e n_i n_e$, where $\sigma_R^* \approx N^{*-2/3} \approx 14\times10^{-16}\ \mathrm{cm^2}$ is the cross section of electron collision with the ionized molecule where nearby electron screens the positive charge, and $p^* \approx n_e/N^*$ is the probability of a second electron being present estimated via the electron density n_e and the molecular density of the crystal N^*. Hence, we can obtain the following expression for this recombination pathway $p^*\sigma_R^* V_e n_i n_e = \beta_R n_i n_e^2$ by using which, we find the following scaling estimate: $\beta_R \approx \sigma_R^* V_e/N^* \approx V_e N^{*-5/3} \approx (7.4\times10^{-31}) - (1.9\times10^{-30})\ \mathrm{cm^6/s}$ for $V_e \approx (1$–$1.25)\times10^7\ \mathrm{cm/s}$ and $N^* \approx 1.9\times10^{22}\ \mathrm{cm^{-3}}$. For Si of density $N^* \approx 5\times10^{22}\ \mathrm{cm^{-3}}$ and the typical range of $V_e \approx (1$–$1.25)\times10^7\ \mathrm{cm/s}$, this scaling gives $\beta_R \approx V_e N^{*-5/3} \approx (1.5$–$3.8)\times10^{-31}\ \mathrm{cm^6/s}$, which agrees well with the experimental value $\beta_R \approx (1$–$3.8)\times10^{-31}\ \mathrm{cm^6/s}$ [38]. By using now the values of $\sigma_R \approx 2\times10^{-14}\ \mathrm{cm^2}$, $\sigma_R^* \approx 14\times10^{-16}\ \mathrm{cm^2}$, we find that for $n_e \approx n_i \approx 2\times10^{17}\ \mathrm{cm^{-3}}$, the ratio of the recombination rates $\beta_R n_i n_e^2/\gamma_R n_i n_e \approx \sigma_R^* n_e/\sigma_R N^* \approx 10^{-6}$ allows us to set $\beta_R = 0$ in all calculations related to our experimental case [32].

IV. RESULTS AND DISCUSSION

A. Analytical approximation

In order to obtain an analytical approximation while retaining the main modification point, we consider the case of $\varepsilon_e \ll E_g$ and $\nu_{e\text{-ph}}^{\mathrm{en}} n_e C_e(T_e - T_L) \ll \gamma_r n_e n_i E_g$ additionally assuming quasineutrality $n_e \approx n_i$. In this case, the 2T model reduces to a set of two equations defining the temperature of the lattice:

$$\rho C\frac{dT_L}{dt} = \gamma_R n_e^2 E_g, \tag{11}$$

$$\frac{dn_e}{dt} = W_{\mathrm{PI}} - \gamma_R n_e^2, \tag{12}$$

where $W_{\mathrm{PI}} = W_{\mathrm{TPA}} = \beta_{\mathrm{TPA}} I_2^2/E_g$ for $t \le \tau_P$ and $W_{\mathrm{PI}} = 0$ for $t > \tau_P$.

This model corresponds to the limiting case when the lattice heating is due only to the effect of the recombination of free electrons combined with the direct transfer of recombination energy to the lattice. The solution of these equations is given by the following set of expressions for $t \le \tau_p$:

$$\Delta n_e(t) = a_n \tanh(a_n\gamma_R t), \tag{13}$$

$$\Delta T_L(t) = a_T\left[\frac{t}{\tau_P} - \frac{\tanh(a_n\gamma_R t)}{a_n\gamma_R\tau_P}\right], \tag{14}$$

and for $t > \tau_P$,

$$\Delta n_e(t) = a_n\frac{\tanh(a_n\gamma_R\tau_P)}{1+\tanh(a_n\gamma_R\tau_P)a_n\gamma_R(t-\tau_P)}, \tag{15}$$

$$\Delta T_L(t) = a_T\left[1 - \frac{1}{a_n\gamma_R\tau_P}\times\frac{\tanh(a_n\gamma_R\tau_P)}{1+\tanh(a_n\gamma_R\tau_P)a_n\gamma_R(t-\tau_P)}\right], \tag{16}$$

where $a_n = [\beta_{\mathrm{TPA}} I_2^2/(E_g\gamma_R)]^{1/2}$ is the characteristic scale of the free electron density, and $a_T = \beta_{\mathrm{TPA}} I_2^2\tau_P/\rho C$ is the characteristic scale of the lattice temperature.

In Fig. 2, we show this solution using the dimensionless values $\Delta n_e/a_n$ and $\Delta T_L/a_T$ vs t/τ_P for $a_n\gamma_R\tau_P \approx 2.6$ corresponding to the experimental case [32]: $a_n \approx 2.7\times10^{17}\ \mathrm{cm^{-3}}$, $\gamma_R \approx 0.53\times10^{-6}\ \mathrm{cm^3/s}$, $\varepsilon_0 = 2\hbar\omega - E_g = 0.2\ \mathrm{eV}$, and $\tau_P \approx 18\ \mathrm{ps}$. A few important points are clear from this solution. First, for TPA ionization, the lattice temperature tends finally towards the value of

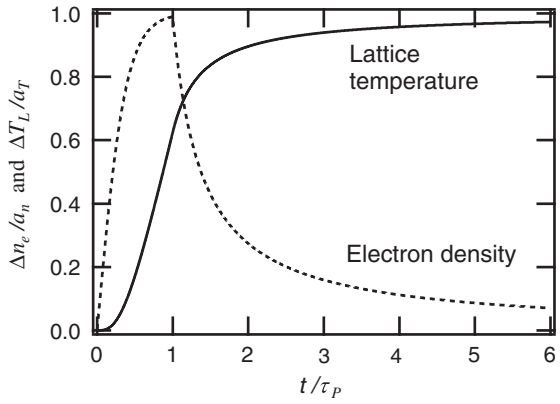

FIG. 2. Analytical solution: The dimensionless electron density and lattice temperature vs time.

$a_T = \beta_{\mathrm{TPA}} I_2^2 \tau_P / \rho C$. Second, the increase of lattice temperature controlled by the rate of recombination does not stop after pulse termination. In particular, only after a period of approximately $5\tau_P \approx 90$ ps does the lattice temperature reach the value of $0.95 a_T$. Third, the characteristic time of recombination can be scaled as follows vs the radiation intensity involved in the process of photoionization $I_2 = \eta I_1$:

$$\tau_R = (a_n \gamma_R)^{-1} = \frac{E_g^{1/2}}{\beta_{\mathrm{TPA}}^{1/2} \gamma_R^{1/2} I_2}. \tag{17}$$

This scaling shows that for the considered case (i) the recombination time depends weakly on the electron energy, i.e., $\tau_R \propto \varepsilon_e^{-1/4}$ and (ii) $\tau_R \propto 1/I_2$ agreeing with the experimental data on after-pulse electron-relaxation dynamics vs the intensity of the ionizing radiation [29].

Finally, in Fig. 3, we show the value of $\{[\Delta T_L(\tau_P)]/a_T\} = 1 - \{[\tanh(a_n \gamma_R \tau_P)]/a_n \gamma_R \tau_P\}$ estimated by Eq. (14) for $t = \tau_P$ as a function of the pulse duration in the range of 100 fs to 1 ns. This figure shows an extent of transfer to the lattice of the energy absorbed by photoionization at the end of the laser pulse, i.e., $\{[\Delta T_L(\tau_P)]/a_T\} = \rho C \Delta T_L(\tau_P)/\beta_{\mathrm{TPA}} I_2^2 \tau_P$. In particular, for $\tau_P < 1$ ps, the lattice remains cold at the end of the laser pulse, whereas for $\tau_P > 0.1$ ns, the laser energy absorbed by photoionization is almost completely transferred to the lattice. Additionally, this figure shows that the time scale of complete electron-lattice equilibration is of order 100 ps.

B. Numerical simulation

Let us now consider the results of simulation showing in full detail how this model operates for the experimental case [32]. We simulate electron excitation, electron-lattice energy transfer, and equilibration on the time scale of $\Delta t = 150$ ps. The ionization rate associated with the TPA of the second harmonic is modeled by $W_{\mathrm{PI}}(n_{\mathrm{ph}}\hbar\omega - E_g) = \beta_{\mathrm{TPA}} I_2^2 (2\hbar\omega_2 - E_g)/E_g$ with $\beta_{\mathrm{TPA}} \approx 2.5$ cm/GW, $2\hbar\omega_2 \approx 4.8$ eV, $E_g = 4.6$ eV, and $I_2 = \eta I_1 \approx 3.32$ GW/cm^2. On the time scale of $\Delta t = 150$ ps, the temperature perturbation does not reach the side surfaces of the crystal with cross section of 2×1 mm, allowing us to use at the side surfaces the condition $E = -\nabla\varphi = 0$, where φ is the electric potential. The values of laser fields are defined by $E_i = (I_i/2n_{\mathrm{RI}}\epsilon_0 c)^{1/2}$, where n_{RI} is the refractive index of $LiTaO_3$ [40].

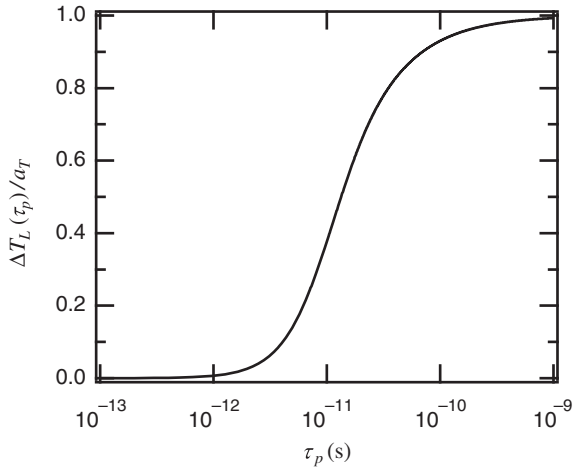

FIG. 3 Analytical solution: Absorbed energy transfer to the lattice at the end of the pulse as a function of the pulse duration.

In computer simulations, we start by using the value $\nu_{e\text{-ph}}^{\mathrm{en}}$ defined as follows: $\nu_{e\text{-ph}}^{\mathrm{en}} = \nu_{e\text{-ph}}^{\mathrm{mom}}(m_e/M_a)^{1/2} \approx 0.14 \times 10^{12}$ Hz ($M_a = 47$ a.u. is the mean atomic mass) and giving $\tau^* = 1/\nu_{e\text{-ph}}^{\mathrm{en}} \approx 7$ ps [15,28]. After that, we simulate the range $\nu_{e\text{-ph}}^{\mathrm{en}} \approx 10^{12} - (2.9 \times 10^{12})$ Hz and $\tau^* = 1/\nu_{e\text{-ph}}^{\mathrm{en}} \approx 0.35 - 1$ ps and discuss related effects. The values $\nu_{e\text{-ph}}^{\mathrm{en}} \approx 10^{12}$ Hz and $\tau^* = 1/\nu_{e\text{-ph}}^{\mathrm{en}} \approx 1$ ps are the generally accepted values for the dielectrics [36,37], whereas the values of $\nu_{e\text{-ph}}^{\mathrm{en}} \approx (1.4 \times 10^{12})$–$(2.9 \times 10^{12})$ Hz and $\tau^* = 1/\nu_{e\text{-ph}}^{\mathrm{en}} \approx 0.35 - 0.7$ ps are estimated from $\nu_{e\text{-ph}}^{\mathrm{en}} = g/(n_e C_e)$, where g is the value of the electron-phonon coupling constant given in W/K cm^3 for silicon-dioxide-like materials [41].

First, we give a set of two figures showing our simulation data for $\tau^* = 1/\nu_{e\text{-ph}}^{\mathrm{en}} \approx 7$ ps. Figure 4(a) shows the charge density, Fig. 4(b) the electron energy, Fig. 4(c) the generated electric field, and Fig. 4(d) the lattice temperature vs time. Figure 4(a) shows that the charge density achieves the saturation level $n_e = [\beta_{\mathrm{TPA}} I_2^2/(E_g \gamma_R)]^{1/2}$, and the electron-ion separation does not happen on the time scale of $\Delta t = 150$ ps.

This result agrees with the estimate of the electron diffusion coefficient $D_e = \mu k_B T_e / e \approx 0.2$ cm^2/s [$\mu \approx 1$ cm^2/V s, $k_B T_e \approx 0.2$ eV, and $E \approx 10^3$ V/cm; see Figs. 4(b) and 4(c)], related diffusion length $(D_e \Delta t)^{1/2} \approx 6 \times 10^{-4}$ mm, and electron drift length $\mu E \Delta t \approx 1.5 \times 10^{-5}$ mm, which are a few orders of magnitude smaller than $\sqrt{2} r_0 = 0.15$ mm. The numerical simulation shown in Fig. 4(a) gives a maximal value of the charge-density approximately 10% lower compared with that given by the analytical approximation, showing that the latter underestimates the increase of the electron energy and of the recombination rate during the pulse. The electron energy shown in Fig. 4(b) increases during the pulse, achieves its maximum of approximately 0.3 eV, decays, and tends with time towards the value defined by the electric field induced in the irradiated zone by the ΔT_L field. The energy of the remaining free electrons $\varepsilon_e \approx 0.3$ eV corresponds roughly to the energy balance of $b|E|(C_e T_e)^{1/2} \approx \nu_{e\text{-ph}}^{\mathrm{en}} C_e (T_e - T_L)$ and is due to the PE field induced by the change of the lattice temperature. However, the contribution of these electrons to the lattice heating is negligibly small because of the low value of n_e reached by the

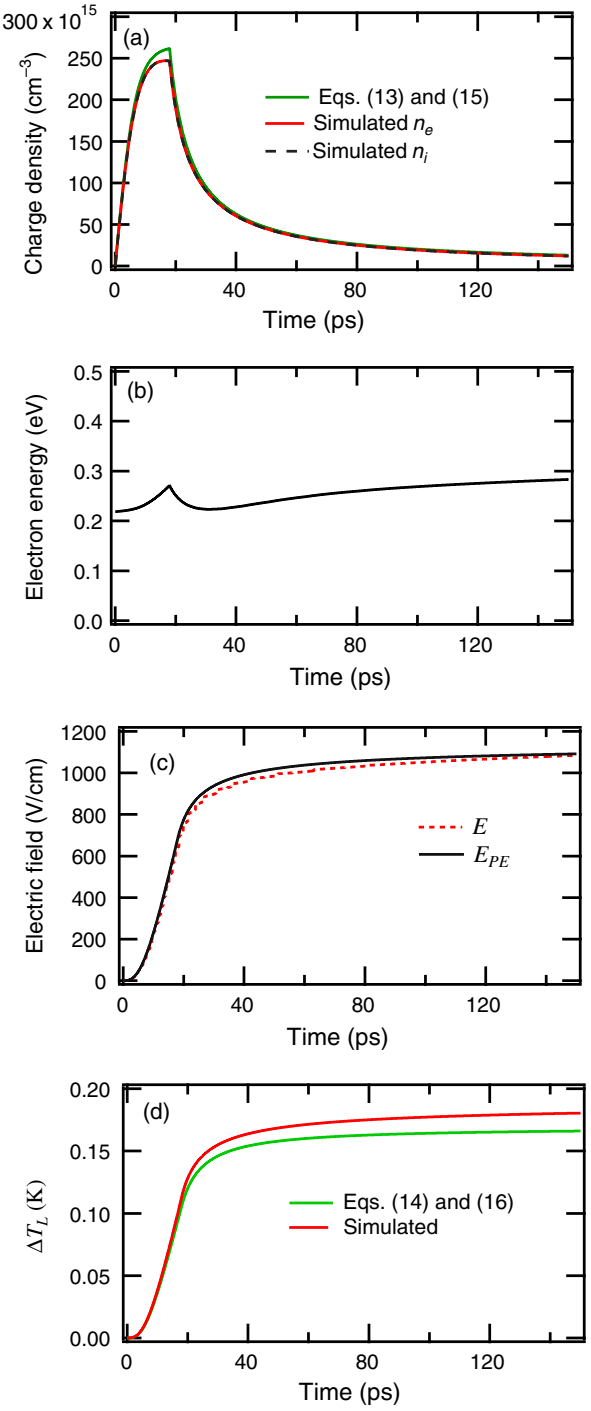

FIG. 4. Simulation of (a) charge density, (b) electron energy, (c) generated electric field, and (d) lattice temperature vs time.

end of the relaxation period when the lattice temperature increase and PE field reach their maxima. Figure 4 shows that the recombination process and thermal relaxation are dominated by the effect of $\gamma_R n_e n_i$ and continue approximately 50 ps after the pulse termination. The onset of the electric field [Fig. 4(c)] corresponds to the time of recombination and electron-lattice relaxation of approximately 50 ps. The effect of charge separation is negligibly small as compared with $E_{\mathrm{PE}} = -[(dP_s)/dT][(\Delta T_L)/\epsilon\epsilon_0]$ induced by the increase of the lattice temperature.

It should be stressed that the simulated temperature of the lattice obtained at the end of the electron-lattice relaxation period [Fig. 4(d)] $\Delta T_L \approx 0.182$ K agrees well with $\Delta T_{\mathrm{SP}} \approx 0.18$ K found from the experiment by Eq. (1). The temperature increase given by the analytical approximation ($\Delta T_L \approx 0.165$ K at $t = 150$ ps) is close to that of the simulation ($\Delta T_L \approx 0.182$ K at $t = 150$ ps). The difference is due to the additional heating of free electrons by two laser waves with the main effect caused by 1030-nm radiation. It is also necessary to note that after pulse termination, the lattice temperature and PE field decay on the time scale of the heat-diffusion effect of order approximately $2r_0^2/D_T \approx 10^{-2}$ s, i.e., by $\Delta T_L \approx [(\beta_{\mathrm{TPA}} I_2^2 \tau_P)/\rho C] \exp(-tD_T/2r_0^2)$, whereas on the time scale of $\Delta t = 150$ ps, the heat-diffusion length $(D_T \Delta t)^{1/2} \approx 1.7 \times 10^{-4}$ mm is about 3 orders of magnitude smaller than $\sqrt{2} r_0 = 0.15$ mm, and the effect of heat diffusion is negligibly small.

Figure 5(a) shows the energy-transfer rates for the electron subsystem, Fig. 5(b) shows the energy-transfer rates for the lattice subsystem, Fig. 5(c) the electron energy density $n_e C_e T_e$, and Fig. 5(d) shows the lattice energy density $\rho C \Delta T_L$. In particular, Fig. 5(a) shows that the rates of all effects involved in electron heating have about the same order of magnitude with maxima around 1–2 GW/cm^3, whereas Fig. 5(b) shows that the lattice heating is mainly due to the effect of $\gamma_R n_e n_i E_g$ providing approximately 90% of the total thermal effect.

In Figs. 6(a)–6(c), we consider the computational results for $\nu_{e-\mathrm{ph}}^{\mathrm{en}} \approx 10^{12}$–$(2.9 \times 10^{12})$ Hz and $\tau^* = 1/\nu_{e\text{-ph}}^{\mathrm{en}} \approx$ 0.35–1 ps, and compare them with those made for $\tau^* = 1/\nu_{e\text{-ph}}^{\mathrm{en}} \approx 7$ ps. In particular, in Fig. 6(a), we show the charge density, Fig. 6(b) the electron energy, and Fig. 6(c) the lattice temperature vs time. Let us outline the significant points. First, for a change from $\tau^* \approx 7$ ps to $\tau^* \approx 1$ ps and $\tau^* \approx 0.35$ ps, the charge density increases on approximately 25% and 40%. This increase is due to the significant decrease of the electron energy (and V_e) shown in Fig. 6(b) caused by a faster energy transfer to the lattice. In particular, for $\tau^* \approx 7$ ps, the electron energy reaches the maximum of approximately 0.3 eV, decays after pulse termination, and tends finally to the level defined by the generated E field. In contrast, for lower values of $\tau^* \approx 1$ ps and $\tau^* \approx 0.35$ ps, the electron energy decays starting from the initial value of approximately 0.2 eV and tending finally to the level defined by the generated E field. However, in all cases, the relaxation time is approximately 50 ps. It should be noted that the final lattice temperature value achieved after full relaxation does not change significantly with decrease of τ^*, remaining in all cases close to 0.18 K. That is, regardless of the value of τ^*, the electron-lattice relaxation is controlled by

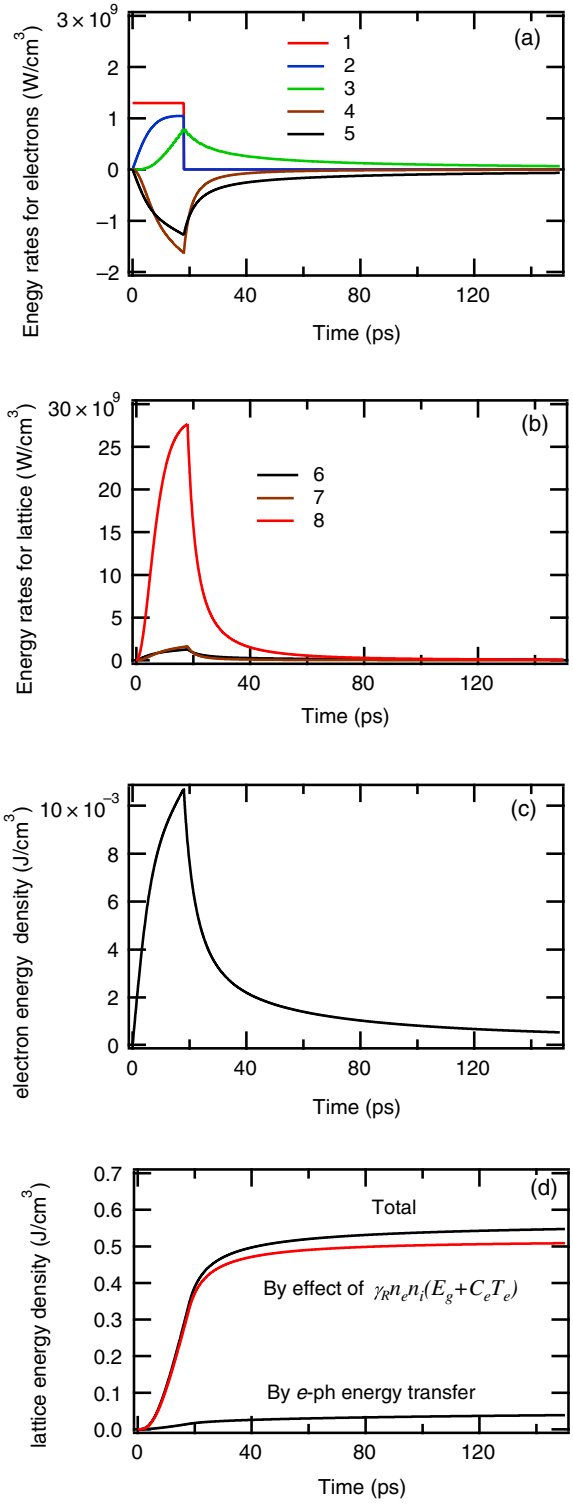

FIG. 5. Simulated energy density data given vs time. (a) Energy rates for the electron subsystem from the following contributions: (1) $\beta_{\mathrm{TPA}} I_2^2 (2\hbar\omega_2 - E_g)$, (2) $n_e \sum 2\varepsilon_{\mathrm{qi}} \nu_{e\text{-ph}}^{\mathrm{mom}}$, (3) $bn_e|E|(C_e T_e)^{1/2}$, (4) $-\gamma_R n_i n_e C_e T_e$, and (5) $-\nu_{e\text{-ph}}^{\mathrm{en}} n_e C_e (T_e - T_L)$. (b) Energy rates for the lattice subsystem: (6) $\gamma_R n_i n_e C_e T_e$, (7) $\nu_{e\text{-ph}}^{\mathrm{en}} n_e C_e (T_e - T_L)$, and (8) $\gamma_R n_i n_e E_g$. (c) Electron energy density $n_e C_e T_e$ and (d) lattice energy density $\rho C \Delta T_L$.

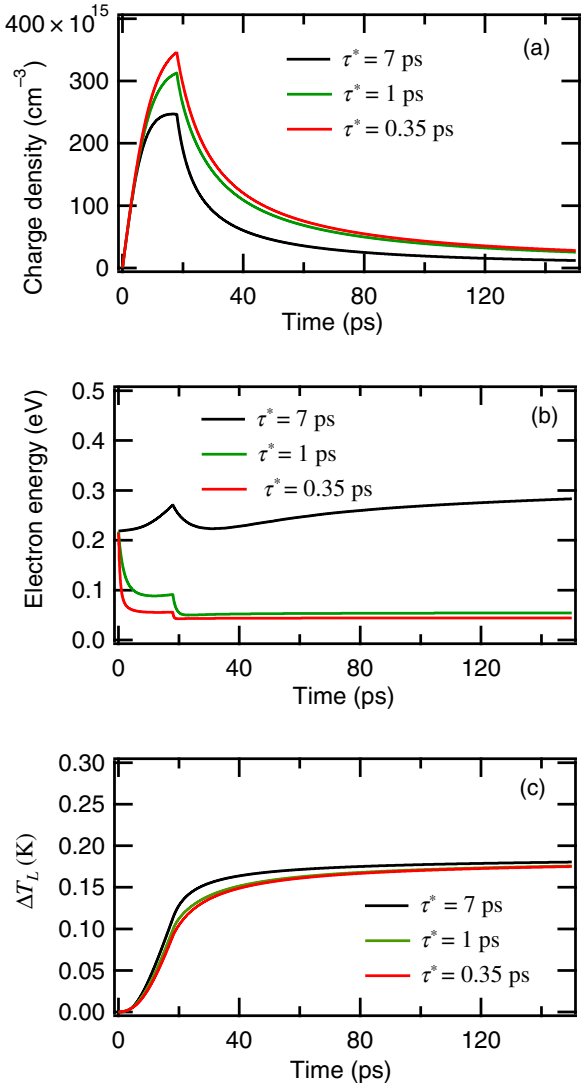

FIG. 6. Simulated data vs time: (a) charge density, (b) energy of free electrons, and (c) lattice temperature resulting after a single pulse.

the recombination stage continuing for approximately 50 ps in all cases, and the thermal effect is dominated by recombination heat release.

Additionally, in Fig. 7 we show the values of the relative energy transfer integrated over the whole period vs the value of τ^* from (i) the effect of recombination heat release of $\gamma_R n_i n_e (E_g + C_e T_e)$ and (ii) the effect mediated by the electron-phonon energy transfer $\nu_{e\text{-ph}}^{\mathrm{en}} n_e C_e (T_e - T_L)$. This figure shows that the energy transfer is dominated by the direct transfer of the recombination energy to the lattice for the whole range of τ^* considered in our study.

We should stress that the relaxation continues for approximately 50 ps after the pulse termination agreeing to an order of magnitude with the experimental observations of electron-lattice relaxation dynamics [26,27,29].

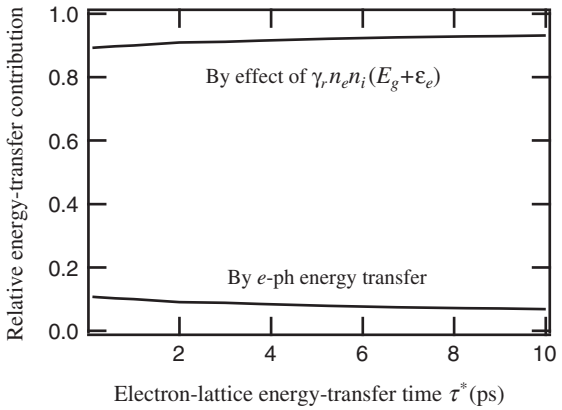

FIG. 7. Relative contributions of energy-transfer effects vs τ^*.

Thus, our computational study suggests that the process of the electron-lattice relaxation is controlled by the recombination-stage bottleneck (approximately 50 ps), which is at least about 1 order of magnitude higher than the characteristic time of the electron-phonon energy transfer (0.3–7 ps).

To finalize this section, we note that the release of recombination heat directly to the lattice is associated with phonon generation required for heat dissipation and taking place during the whole period of recombination, which agrees well with the observations [27,28] where approximately (15–50)–ps phonon generation under femtosecond-laser-induced plasma relaxation in the bulk of crystalline insulators is found.

V. ADDITIONAL REMARKS

The experiment, theoretical model, and simulation that we consider here show that this case corresponds to the low charge density combined with low electron energy in which the generated thermal effect is mainly due to the recombination heat release into the lattice. We suggest that this pathway of energy transfer to the lattice is able also to play a significant role in combination with other effects in many processes of laser-matter interaction in dielectrics and semiconductors.

In particular, this modification can be used for the theoretical treatment of other applications in which the irradiated dielectrics are close to full ionization with high charge density of approximately 10^{22} cm^{-3} and high electron energies inducing avalanche ionization. It is important to note here that the involvement of $\beta_R n_i n_e^2$ in the recombination process can lead to (i) a significant increase of electron energy followed by (ii) a faster energy transfer to the lattice due to electron-phonon energy transfer. Under combined recombination occurring when the electron density and energy vary with time, the recombination time can exhibit a more complex character. In particular, considering the relaxation by using $dn_e/dt = -\gamma_R n_e^2$, one finds that the process of after-pulse relaxation is defined by $n_e(t) \approx n_{\max}/(1 + n_{\max}\gamma_R t)$, where $n_{\max}$ is the maximal electron density reached at the end of the laser pulse. By using $dn_e/dt = -\beta_R n_e^3$, one finds that the relaxation is defined by $n_e(t) \approx n_{\max}/(1 + 2n_{\max}^2\beta_R t)^{1/2}$. However, unlike the case considered in our study, under high densities of charges generated by photoionization and related characteristic recombination time of approximately $(\beta_R n_{\max}^2)^{-1} \ll \tau^* \approx 1$ ps, the laser-matter energy transfer is hindered by the electron-phonon energy-transfer rate.

In considering this case, we should note that even under laser intensities inducing avalanche ionization, the electrons are not able to achieve energy much above the level of E_g because after reaching this energy level, the electrons are involved in impact ionization losing E_g per every ionizing collision with lattice atoms. Hence, even in high-intensity laser interaction under avalanche ionization, the effect of recombination energy release to the lattice suggested here can provide an effective pathway to the total energy transfer to the lattice and electron-lattice relaxation. To treat these operational conditions with $\varepsilon_e > 1.5E_g$, our modification should be properly combined with kinetic and thermal effects of electron avalanche ionization [18,24,25]. In particular, the model should include the value of $R_i n_e$ in electron-ion rate equations and the value of electron energy loss $-R_i n_e E_g$ in the electron energy rate equation (R_i is the frequency of impact ionization).

Additionally, in using this modification for other cases of high-intensity laser-matter interaction, one should take into account several significant effects. First, under high charge density, the Coulomb cross section σ_R used in $\gamma_R = \sigma_R V_e$ is significantly reduced by the screening effect, tending to that of $\sigma_R^* \approx (N^*)^{-2/3} \approx 14 \times 10^{-16}$ cm^2. The screening effect should be also taken into account in treating Auger recombination when $n_e > 10^{21}$ cm^{-3} [42]. Second, for n_e reaching closely to the range of 10^{21}–10^{22} cm^{-3}, the crystalline state of the irradiated matter is no longer a thermodynamically stable phase [42]. Third, under high charge density, high electron, and lattice temperature, the band-gap energy can be reduced [43], leading to a significant enhancement of absorption-, photo-, collision-, and thermally induced ionization rates. Fourth, with increase in charge density when $(\gamma_R n_e)^{-1} \approx \tau^*$, the relaxation process is controlled by e-ph energy transfer. In order to treat this effect, the related recombination rate used in this model $\gamma_R n_i n_e$ should be modified as follows: $n_e/[\tau^* + (\gamma_R n_i)^{-1}]$ [42].

Finally, we note that the suggested mechanism and theoretical treatment can be used for developing computational techniques for simulation of short-pulsed laser-beam propagation in nonlinear laser-frequency conversion prone to various effects of photoionization. In particular, the generation of the free electrons can produce a significant change of refractive indices for the laser beams

$\Delta n_{\mathrm{RI}} \approx -\omega_p^2/2\omega_i^2$. The change of the refractive indices can lead to a loss of initial phase-matching condition in periodically poled structures $\Delta k = 2k_1 - k_2 - 2\pi/\Lambda = 0$ [1], where $k_i = n_{\mathrm{RI}}\omega_i/c$ are the values of wave vectors, and Λ is the poling period. A laser beam propagating across the medium with a nonuniform distribution of the refractive index can experience a strong lensing effect leading to an additional mismatch Δk, dephasing effect, and beam distortions [1].

The modifications suggested here can be used for developing a more comprehensive framework for the simulation of electron density and electron energy coupled with the integration of a laser-beam propagation model under filamentation in optical crystals [44]. Our inclusion of the recombination heat release to the lattice can be also extended (with appropriate modifications taking into account relevant energy levels) to the photoionization-recombination kinetics, laser-beam filamentation, and electron-lattice relaxation via the interband energy levels and related defects known to exist in optical crystals [14,29,44]. However, a detailed consideration of these effects and related electron kinetics in multilevel complex energy systems is out of the scope of the present study.

VI. SUMMARY

To conclude, this work suggests a modification of the 2T model for treating short-pulsed laser-matter interaction in nonlinear optical crystals based on the estimation of single-pulse temperature increase obtained from the experimental data of the temperature-controlled picosecond-pulsed SHG in PPSLT crystal. We show that for the considered experimental case, the main mechanism of the lattice heating after generation of free electrons via the two-photon absorption of generated second harmonic is due to the recombination mechanism combined with the direct transfer of the recombination energy to the lattice subsystem. The effect of this mechanism provides approximately 90% of laser-matter energy transfer and extends for approximately 50 ps after laser-pulse termination due to a recombination-stage bottleneck which hinders a faster relaxation to the thermal equilibrium. Generally, our model and detailed computational study suggest that under photoionization by short-pulsed radiation with intensity range used in nonlinear laser-frequency conversion, the electron-lattice relaxation is controlled by the recombination-stage bottleneck and not by the characteristic time of electron-phonon energy transfer.

We consider a modification of the 2T model directly suitable for the relatively low laser intensities used in nonlinear laser-frequency conversion processes when the energies achieved by the free electrons are not sufficient for the onset of collisional electron avalanche ionization. However, our estimates suggest that this modification combined with the formalism for avalanche ionization can be expanded to other applications using significantly higher laser intensities. Under high intensity, short-pulsed laser interaction with dielectrics, and high electron density generated during the pulse, this pathway of recombination with direct energy transfer to the lattice can also provide a significant contribution to the total laser-matter energy-transfer mechanism.

This 2T model can be combined with the formalisms of nonlinear laser-frequency conversion allowing a comprehensive simulation and optimization of operational and device parameters involved in short-pulsed nonlinear laser-frequency conversion techniques. In particular, this model can be used for the simulation of the fields of the electron density, electron, and lattice temperatures enabling the calculation of the threshold laser intensities under which the operation can be strongly inhibited by thermal or electron dephasing or completely disabled by laser-induced crystal damage. This model can be also used for estimating the temperature range necessary for temperature-controlled operation of the crystal and process optimization for specific application-oriented devices using nonlinear laser-frequency conversion. We also note that developed analytical approximation for electron-lattice relaxation with appropriate modifications can be also used for the case of multiphoton absorption.

Finally, we suggest here that the effect of energy transfer to the lattice during photoionization and relaxation can play a significant role in other processes of laser-matter interaction including modification of the optical properties, ablation, phenomena of optical breakdown, damage, and short-pulsed filamentation.

ACKNOWLEDGMENTS

We like to thank Dr. J. Hester (ANSTO, Australia) and Dr. A. S. Mishchenko (RIKEN, Japan) for helpful discussions on the subject of this work, reading the manuscript, and providing many comments. Special thanks are addressed to the anonymous referees of this paper for providing very valuable and detailed feedback for our work.

[1] R. W. Boyd, *Nonlinear Optics*, 3rd ed. (Academic Press, New York, 2008), and references therein.
[2] M. Yamada, N. Nada, M. Saitoh, and K. Watanabe, First-order quasi-phase matched $LiNbO_3$ waveguide periodically poled by applying an external field for efficient blue second-harmonic generation, Appl. Phys. Lett. **62**, 435 (1993).
[3] R. L. Byer, Quasi-phasematched nonlinear interactions and devices, J. Nonlinear Opt. Phys. Mater. **06**, 549 (1997).
[4] J. A. Armstrong, N. Bloembergen, J. Ducuing, and P. S. Pershan, Interactions between light waves in a nonlinear dielectric, Phys. Rev. **127**, 1918 (1962).
[5] V. Pasiskevicius, G. Strömqvist, F. Laurell, and C. Canalias, Quasi-phase matched nonlinear media: Progress towards nonlinear optical engineering, Opt. Mater. **34**, 513 (2012).

[6] O. A. Louchev, N. E. Yu, S. Kurimura, and K. Kitamura, Thermal inhibition of high power second harmonic generation in periodically poled $LiNbO_3$ and $LiTaO_3$ crystals, Appl. Phys. Lett. **87**, 131101 (2005).

[7] O. A. Louchev, N. E. Yu, S. Kurimura, and K. Kitamura, Nanosecond pulsed laser energy and thermal field evolution during second harmonic generation in periodically poled $LiNbO_3$ crystal, J. Appl. Phys. **98**, 113103 (2005).

[8] S. G. Sabouri and L. Khorsandi, Thermal dephasing compensation in high-power and high-repetition-rate second-harmonic generation using spillover loss, J. Opt. Soc. Am. B **33**, 1640 (2016).

[9] M. I. Kaganov, I. M. Lifshitz, and M. V. Tanatarov, Relaxation between electrons and the crystalline lattice, Sov. Phys. JETP **4**, 173 (1957).

[10] S. I. Anisimov, B. L. Kapeliovich, and T. L. Perel'man, Electron emission from metal surfaces exposed to ultrashort laser pulses, Sov. Phys. JETP **39**, 375 (1974).

[11] S. A. Akhmanov, V. I. Emel'yanov, N. I. Koroteev, and V. N. Seminogov, Interaction of powerful laser radiation with the surfaces of semiconductors and metals: Nonlinear optical effects and nonlinear optical diagnostics, Sov. Phys. Usp. **28**, 1084 (1985).

[12] H. M. van Driel, Kinetics of high-density plasmas generated in Si by 1.06- and 0.53-μm picosecond laser pulses, Phys. Rev. B **35**, 8166 (1987).

[13] P. B. Corkum, F. Brunel, N. K. Sherman, and T. Srinivasan-Rao, Thermal Response of Metals to Ultrashort-Pulse Laser Excitation, Phys. Rev. Lett. **61**, 2886 (1988).

[14] S. C. Jones, P. Braunlich, R. T. Aasper, X. A. Shen, and P. Kelly, Recent progress on laser-induced modifications and intrinsic bulk damage of wide-gap optical materials, Opt. Eng. (Bellingham, Wash.) **28**, 1039 (1989).

[15] E. G. Gamaly, *Femtosecond Laser-Matter Interaction: Theory, Experiments and Applications* (Pan Stanford, Singapore, 2011), and references therein.

[16] M. Z. Alam, I. De Leon, and R. W. Boyd, Large optical nonlinearity of indium tin oxide in its epsilon-near-zero region, Science **352**, 795 (2016).

[17] D. Arnold and E. Cartier, Theory of laser-induced free-electron heating and impact ionization in wide-band-gap solids, Phys. Rev. B **46**, 15102 (1992).

[18] B. C. Stuart, M. D. Feit, A. M. Rubenchik, B. W. Shore, and M. D. Perry, Laser-Induced Damage in Dielectrics with Nanosecond to Subpicosecond Pulses, Phys. Rev. Lett. **74**, 2248 (1995).

[19] B. C. Stuart, M. D. Feit, A. M. Rubenchik, B. W. Shore, and M. D. Perry, Optical ablation by high-power short-pulse lasers, J. Opt. Soc. Am. B **13**, 459 (1996).

[20] M. Lenzner, J. Krüger, S. Sartania, Z. Cheng, Ch. Spielmann, G. Mourou, W. Kautek, and F. Krausz, Femtosecond Optical Breakdown in Dielectrics, Phys. Rev. Lett. **80**, 4076 (1998).

[21] A. Kaizer, B. Rethfeld, M. Vicanek, and G. Simon, Microscopic processes in dielectrics under irradiation by subpicosecond pulses, Phys. Rev. B **61**, 11437 (2000).

[22] K. Eidmann, J. Meyer-ter-Vehn, T. Schlegel, and S. Hüller, Hydrodynamic simulation of subpicosecond laser interaction with solid-density matter, Phys. Rev. E **62**, 1202 (2000).

[23] E. G. Gamaly, A. V. Rode, B. Luther-Davies, and V. T. Tikhonchuk, Ablation of solids by femtosecond lasers: Ablation mechanism and ablation thresholds for metals and dielectrics, Phys. Plasmas **9**, 949 (2002).

[24] B. Rethfeld, Unified Model for the Free-Electron Avalanche in Laser-Irradiated Dielectrics, Phys. Rev. Lett. **92**, 187401 (2004).

[25] B. Rethfeld, Free electron generation in laser-irradiated dielectrics, Phys. Rev. B **73**, 035101 (2006).

[26] V. M. Gordienko, F. V. Potemkin, and P. M. Mikheev, Evolution of a femtosecond laser-induced plasma and energy transfer processes in SiO_2 microvolume detected by the third harmonic generation technique, JETP Lett. **90**, 263 (2009).

[27] V. M. Gordienko, P. M. Mikheev, and F. V. Potemkin, Generation of coherent terahertz phonons by sharp focusing of a femtosecond laser beam in the bulk of crystalline insulators in a regime of plasma formation, JETP Lett. **92**, 502 (2010).

[28] E. G. Gamaly, S. Juodkazis, V. Mizeikis, H. Misawa, A. V. Rode, and W. Krolikowski, Modification of refractive index by a single femtosecond pulse confined inside a bulk of photorefractive crystal, Phys. Rev. B **81**, 054113 (2010).

[29] G. Duchateau, G. Geoffroy, A. Dyan, H. Piombini, and S. Guizard, Electron-hole dynamics in normal and deuterated KH_2PO_4 illuminated by intense femtosecond laser pulses, Phys. Rev. B **83**, 075114 (2011).

[30] L. Gallais, D.-B. Douti, M. Commandré, G. Batavičiūtė, E. Pupka, M. Ščiuka, L. Smalakys, V. Siutkaitis, and A. Melninkaitis, Wavelength dependence of femtosecond laser-induced damage threshold of optical materials, J. Appl. Phys. **117**, 223103 (2015).

[31] N. M. Bulgakova, V. P. Zhukov, S. V. Sonina, and Yu. P. Meshcheryakov, Modification of transparent materials with ultrashort laser pulses: What is energetically and mechanically meaningful?, J. Appl. Phys. **118**, 233108 (2015).

[32] O. A. Louchev, H. Hatano, T. Tsukihana, S. Wada, S. Takekawa, and K. Kitamura, Temperature-controlled picosecond-pulsed high frequency second-harmonic generation by a periodically poled stoichiometric $LiTaO_3$, Opt. Express **23**, 4847 (2015).

[33] O. A. Louchev, H. Hatano, S. Wada, and K. Kitamura, Optical breakdown threshold in nanosecond high repetition second harmonic generation by periodically poled Mg-doped $LiTaO_3$ crystal, Appl. Phys. Lett. **103**, 091114 (2013).

[34] O. A. Louchev, H. Hatano, N. Saito, S. Wada, and K. Kitamura, Laser-induced breakdown and damage generation by nonlinear frequency conversion in ferroelectric crystals: Experiment and theory, J. Appl. Phys. **114**, 203101 (2013).

[35] M. Nakamura, S. Takekawa, and K. Kitamura, Thermal diffusivity along x-axis of periodically poled Mg-doped near-stoichiometric $LiTaO_3$ device with domain-inverted period of 8.0 μm, Jpn. J. Appl. Phys. **51**, 012601 (2012).

[36] N. M. Bulgakova, R. Stoian, A. Rosenfeld, I. V. Hertel, W. Marine, and E. E. B. Campbell, A general continuum approach to describe fast electronic transport in pulsed laser irradiated materials: The problem of Coulomb explosion, Appl. Phys. A **81**, 345 (2005).

[37] N. M. Bulgakova, R. Stoian, A. Rosenfeld, I. V. Hertel, and E. E. B. Campbell, in *Laser Ablation and Its Applications*,

edited by C. Phipps, Springer Series in Optical Sciences Vol. 129 (Springer, New York, 2007), pp. 16–36.

[38] J. Dziewior and W. Schmid, Auger coefficients for highly doped and highly excited silicon, Appl. Phys. Lett. **31**, 346 (1977).

[39] P. Martin, S. Guizard, Ph. Daguzan, G. Petite, P. D'Oliveira, P. Meynadier, and M. Pedrix, Subpicosecond study of carrier trapping dynamics in wide-band-gap crystals, Phys. Rev. B **55**, 5799 (1997).

[40] A. Bruner, D. Eger, M. B. Oron, P. Blau, M. Katz, and S. Ruschin, Temperature-dependent Sellmeier equation for the refractive index of stoichiometric lithium tantalite, Opt. Lett. **28**, 194 (2003).

[41] N. Brouwer and B. Rethfeld, Excitation and relaxation dynamics in dielectrics irradiated by an intense ultrashort laser pulse, J. Opt. Soc. Am. B **31**, C28 (2014).

[42] J. Bok and M. Combescot, Comment on the "Evidence for a Self-Confined Plasma" in Laser Annealing, Phys. Rev. Lett. **47**, 1564 (1981), and references therein.

[43] J. A. Van Vechten and M. Wautelet, Variation of semiconductor band gaps with lattice temperature and with carrier temperature when these are not equal, Phys. Rev. B **23**, 5543 (1981).

[44] J. Rolle, L. Bergé, G. Duchateau, and S. Skupin, Filamentation of ultrashort laser pulses in silica glass and KDP crystals: A comparative study, Phys. Rev. A **90**, 023834 (2014).